Extended Abstracts of the 2012 International Conference on Solid State Devices and Materials, Kyoto, 2012, pp460-461

Influence of stacking faults and surface morphology in triangular defects on 4H-SiC junction barrier Schottky diodes

Kazuya Konishi[1], Shuhei Nakata[1], Yoshiyuki Nakaki[1], Yukiyasu Nakao[1], Akemi Nagae[1], Takanori Tanaka[1], Yoshihiko Toyoda[1], Hiroaki Sumitani[2] , and Tatsuo Oomori[2]

[1] Advanced Technology R&D Center, Mitsubishi Electric Corporation,
8-1-1 Tsukaguchi-honmachi, Amagasaki, HYOGO 661-8661, Japan
[2] Power Device Works, Mitsubishi Electric Corporation,
1-1-1 Imajuku-higashi, Nishi-ku Fukuoka, FUKUOKA 819-0192, Japan
Phone: +81-6-6497-7082 E-mail address:Konishi.Kazuya@ct.MitsubishiElectric.co.jp

1. Introduction

In SiC power devices, existence of crystal defects causes increase in the leakage current and decrease in the breakdown voltage[1-3]. Throughout earlier investigations, crystal defects that have significant effects on devices have been identified[4,5]. But some triangular defects affect device performance while the other does not, these reason are not known. Further investigations must be carried out to classify them. The mechanism of the increasing current by a triangular defect is considered to be due to concentration of electric field caused by surface morphology and lowering the barrier height by stacking faults (SFs) of triangular defects[6]. In this study, the relationship between surface morphology or stacking faults and the position of the leakage current inside the triangular defect was analyzed.

2. Experiments

In this report, the evaluation element as SiC-JBS (junction barrier Schottky diode) was fabricated on a 4H-SiC N-type wafer. Before fabrication, we conducted the wafer inspection and obtained the optical microscope images of the triangular defects to evaluate the surface morphology of them and also the location of them to choice the devices including triangular defects to study them. After fabrication, we evaluated the I-V characteristics of these devices. Then, in order to give the evidence to prove that the leakage source is the triangle defect, we located the point of the leakage current inside the triangular defects using a lock-in infrared camera. We also investigated the SFs inside the triangular defects by photoluminescence (PL) mapping and spectropy[7,8] to evaluate the crystal structure at the point of the leakage current inside the triangular defects.

3. Results & Discussion

The I-V characteristics of devices with and without triangular defects were measured. Figure 1 shows the reverse I-V characteristics and Fig. 2 shows the forward I-V characteristics. The defects are categorized into three types A, B, and C based on the IV characteristics. For type A, increase in the leakage current was observed under both forward and reverse biases. For type B, decrease in the breakdown voltage was observed but forward characteristics to not influenced, and for type C, influence of defects is not observed.

The optical microscope images of the triangular defects in these devices are shown in Fig. 3. Types A and C are acute triangles and type B is an obtuse-angle triangle. the triangle defect of type A has convex apex, types B and C have concave apex and the concave of type B looks deeper than type C from the contrast intensity, which indicated that the apex of type B was expected as the concentration point of electric field.

Figure 4 shows the IR images of type A, Fig. 4(a) is an image under reverse bias V_R = 50 V and Fig. 4(b) is under forward bias V_f = 0.65 V. The hot spot is the part in which temperature rises by heat generation of the leakage current and it is located at the base of the triangular defect. In type B and C, hot spot was not observed.

Figure 5 shows the photoluminescence image of stacking faults at 420nm, 460nm, 480nm, and 750nm. In type A, the stacking fault is observed as a dark area at every wavelength. This indicated which the PL peak of SFs exists at the other wavelength. In type B, the device is destroyed during the measurement, and the breaking point is at the apex of a triangular defect. The PL emission contrast inside the triangular defect is not observed and it is thought that any stacking fault is not included inside. In type C, the SF is observed as a bright area at 460nm.

Figure 6 shows the photoluminescence spectrum of SFs of type A and C. In type A, The PL spectrum peak is not observed at every wavelength and the crystal structure is not 4H but the polytype of the SF is unknown now. In type C, the PL spectrum peak of type C is observed at 460nm and this peak corresponds to the near band edge emission of 8H. Thus, the SF of type C is an 8H structure[9,10].

As for type A, It is found that increase in the leakage current was observed under both forward and reverse biases and the leakage source is located at the base of the triangular defect, where the triangular defects has the stacking fault. These results suggest that the some kind of the SF inside the triangular defect causes increase in the leakage current and the mechanism of the increasing current is considered to be lowering the barrier height at the junction of the SF than that of 4H.

As for type B, it is found that decrease in the breakdown voltage was observed and the remarkable concave apex of the triangular defect corresponds to the breaking point.

Thus, the triangular defect including the remarkable concave apex lowers breakdown voltages. This is considered to be caused by the electric field concentrates on the concave apex[11].

4. Conclusions

The relationship between surface morphology or stacking faults and the position of the leakage current inside the triangular defect were analyzed. The defects are categorized into three types based on the IV characteristics. It was found that the some kind of the SF inside the triangular defect causes increase in the leakage current while the other SF such as 8H does not lead deterioration of the device performance in this case. It was also found that including a remarkable concave apex lowers breakdown voltages.

5. Acknowledgements

This work is partially supported by the NEDO project "Novel Semiconductor Power Electronics Project Realizing Low Carbon-emission Society".

6. References

[1] P. N. Neudeck, Mater. Sci. Forum **338–342**, 1161 (2000).
[2] Y. Wang *et al*., J. Appl. Phys. **97**, 013540 (2005).
[3] T. Kimoto *et al*., IEEE Trans. Electron Devices.**46**, 471 (1999).
[4] R. A. Berechman *et al*., J. Appl. Phys. **105**, 074513 (2009).
[5] H. Fujiwara *et al*., Mater. Sci. Forum **679–680**, 694 (2011).
[6] A. O. Konstantinov *et al*., J. Crystal Growth **178,** 495-504 (1997).
[7] M. Tajima *et al*., Appl. Phys. Lett. **86,** 061914 (2005).
[8] G. Feng *et al*., J. Appl. Phys.**94,** 091910 (2009).
[9] W. H. Backes *et al*., J. Appl. Phys.**49,** 7564 (1994).
[10] S. Limpijumnong *et al*., J. Appl. Phys.**59,** 12890 (1999).
[11]T. Katsuno *et al*., J. Appl. Phys. **98,** 222111 (2011).

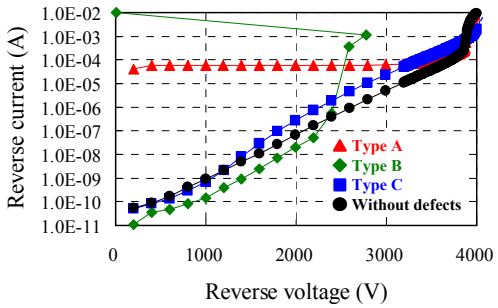

Fig. 1. Reverse current-voltage characteristics.

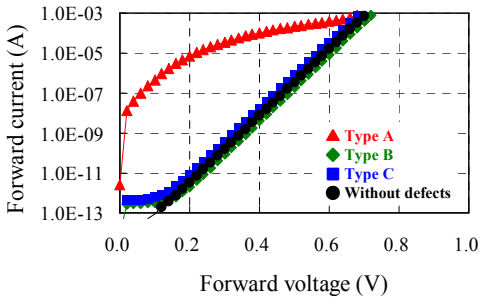

Fig. 2. Forward current-voltage characteristics.

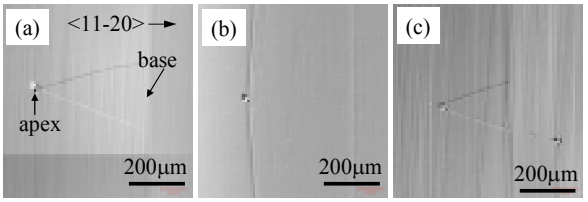

Fig. 3. Optical microscope images of (a) type A defect, (b) type B defect, and (c) type C defects.

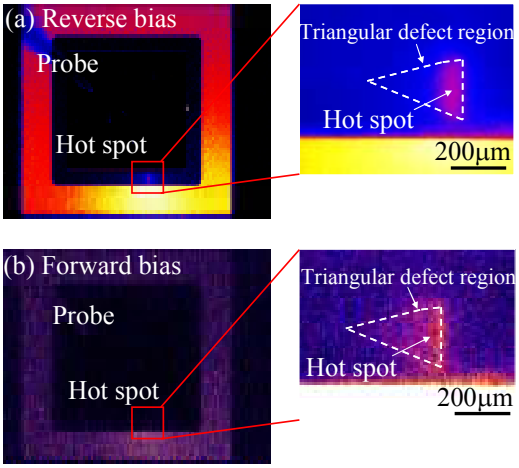

Fig. 4. IR image of type A device (a) at reverse bias V_R = 50 V and (b) at forward bias V_f = 0.65 V.

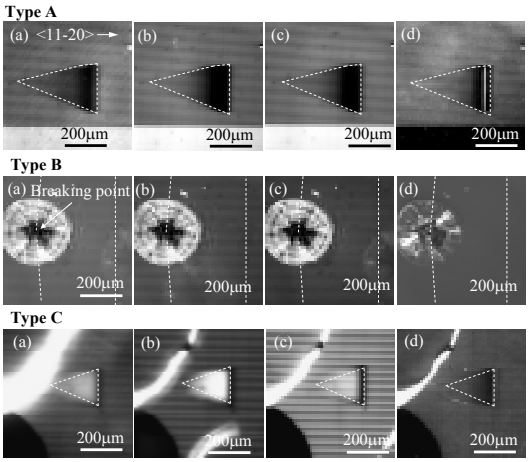

Fig. 5. PL images of each type defects at (a) 420nm, (b) 460nm, (c) 480nm, and (d) 750nm.

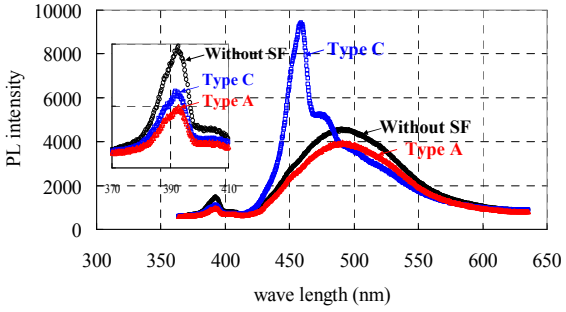

Fig. 6. PL spectrum at RT. The inset indicates the PL spectrum at 370nm - 410nm.